NANO LETTERS

Letter

pubs.acs.org/NanoLett

Edge Mode Coupling within a Plasmonic Nanoparticle

Franz-Philipp Schmidt,*[,†,‡] Harald Ditlbacher,[†] Andreas Hohenau,[†] Ulrich Hohenester,[†] Ferdinand Hofer,[‡] and Joachim R. Krenn[†]

[†]Institute of Physics, University of Graz, 8010 Graz, Austria

[‡]Institute for Electron Microscopy and Nanoanalysis, Graz University of Technology, 8010 Graz, Austria

Supporting Information

ABSTRACT: The coupling of plasmonic nanoparticles can strongly modify their optical properties. Here, we show that the coupling of the edges within a single rectangular particle leads to mode splitting and the formation of bonding and antibonding edge modes. We are able to unambiguously designate the modes due to the high spatial resolution of electron microscopy-based electron energy loss spectroscopy and the comparison with numerical simulations. Our results provide simple guidelines for the interpretation and the design of plasmonic mode spectra.

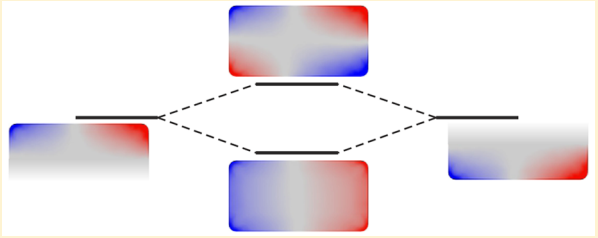

KEYWORDS: *Plasmonics, electron energy loss spectroscopy, transmission electron microscopy, nanoparticles*

The optical properties of noble metal nanostructures are dominated by surface plasmons, giving rise to resonantly enhanced and strongly confined optical fields. Plasmon modes can interact via their fields, leading to coupling-induced effects such as mode splitting and particularly high intensities in small gaps.[1−4] These effects considerably widen the range of the spectral and spatial plasmonic tunability. Accordingly, a thorough theoretical understanding of coupling has been developed, making available effective simulation tools. However, for the understanding of the underlying physics it is often benefical to apply simple models that provide intuitive and general design rules. The hybridization model for coupled plasmon modes provides such rules for arbitrary geometries, enabling an effective ordering of plasmonic modes.[5] A general geometric interpretation of plasmon modes in single nanoparticles was applied to interpret their scattering, including anomalous effects.[6] For flat nanostructures it was shown that the full mode spectrum can be decomposed into elementary surface and edge modes.[7,8] Along these lines, we show in this Letter that a simple coupling model of edge modes within single, rectangular, flat nanoparticles can effectively describe the observed plasmonic mode spectrum.

We investigate the plasmonic properties of silver nanoparticles with a rectangular footprint (cuboids) by electron energy loss spectroscopy (EELS) in a scanning transmission electron microscope (STEM).[9,10] The cuboids with 300−500 nm length, 150 nm width, and 30 nm height (thus suppressing effective coupling between the upper and lower particle interfaces) are fabricated by electron beam lithography on 15 nm thick Si_3N_4 substrates.[7] Electron energy loss (EEL) spectra are acquired in a FEI Tecnai F20 STEM with a monochromated 200 keV electron beam of 150 meV energy spread. All EEL data are deconvolved using the Richardson-Lucy algorithm (Methods section).

In Figure 1a, three EEL spectra acquired at three different positions along the long cuboid edge (1−3, as marked in the electron micrograph in the inset, edge length 300 nm; for other edge lengths see Supplementary Figure 1) are depicted. Apart from the bulk (B) and the asymptotic edge (L) and film (F) peaks,[7,11] we identify pairs of position-dependent peaks, L_1−L_3 and L_1'−L_3'. We note that these modes are localized at the

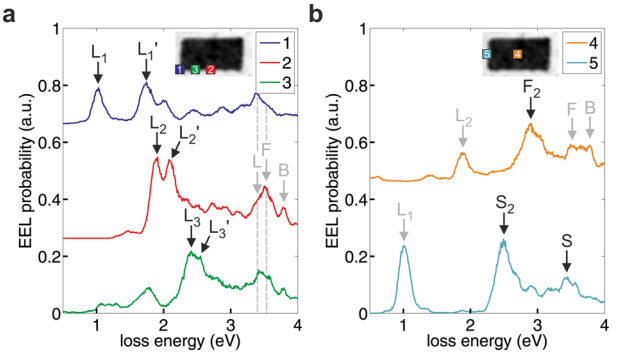

Figure 1. Deconvolved EEL spectra of cuboid edge and film modes. (a) Spectra taken along the long cuboid edge (length 300 nm), as indicated by the numbers in the inset electron micrograph. L_x and L_x' (x = 1, 2, 3) are the edge modes along the long cuboid axis of first to third order, and L is the corresponding asymptotic edge mode. (b) Spectra taken along the short edge and from the cuboid center. S_2 is the second order edge mode along the short cuboid axis, F_2 is the second order film mode along the short cuboid axis, and S is the corresponding asymptotic edge mode. In both panels, F is the asymptotic film mode and B is the bulk plasmon mode.

Received: May 24, 2016
Revised: July 15, 2016
Published: July 18, 2016

DOI: 10.1021/acs.nanolett.6b02097
Nano Lett. 2016, 16, 5152−5155

silver/Si_3N_4 (lower) interface.[7] While indications of the corresponding modes at the silver/air (upper) interface are present on the high energy side of the spectra they are strongly obscured by the bulk and asymptotic film and edge modes.[7] Further features in the spectra in Figure 1a can be attributed to higher order edge and film modes, as discussed in refs 12 and 13. EEL maps taken at the respective peak energies (Figure 2a)

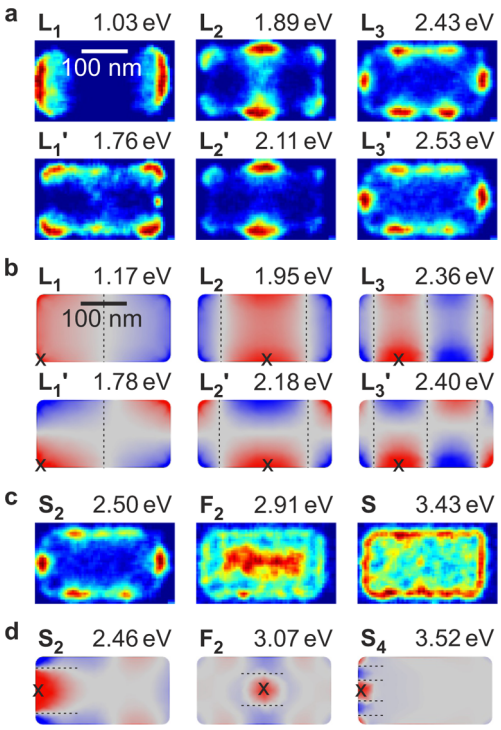

Figure 2. Measured EEL maps and simulated surface charge densities of a cuboid 300 nm long. EEL maps for (a) edge modes along the long cuboid axis and (c) edge and film modes along the short cuboid axis are shown for loss energies as indicated (energy window 100 meV), corresponding to the peak energies in Figure 1. The simulated maps in (b,d) show the corresponding surface charge densities, and the position of the exciting electron beam is marked by the crosses. The dashed lines mark the relevant node lines, aiding the classification of the modes.

help to clarify the nature of these modes. Along the long cuboid edge, we observe two loss maxima at the corners (L_1, L_1'), one additional maximum (L_2, L_2') and two additional maxima (L_3, L_3') on the edges, consistent with standing wave edge modes of first to third order. The maps taken at the two peak energies of a given mode show different patterns apart from the third order peaks. The corresponding maps for the edge lengths of 350, 400, and 500 nm are depicted in Supplementary Figure 2.

At first view the appearance of pairwise peaks and different EEL map patterns for each edge mode order is somewhat puzzling. As detailed in the following, we interpret these observations as coupling of plasmonic modes on opposite cuboid edges, giving rise to bonding and antibonding edge modes. This coupling is prominent in the cuboid structure, as the edge modes are strongly reflected from the cuboid corners. The individual edges act as oscillators of their own and give rise to the observed standing wave patterns. This is in strong contrast to, for example, disk-like nanoparticles where the resonant edge mode condition is dictated by the full disk circumference.[12]

We now compare our experimental results to simulations done with the MNPBEM toolbox, based on the boundary element approach.[14,15] To illustrate the mode patterns, we plot the surface charge densities on the cuboids (for fixed positions of the electron beam) rather than EEL maps.[12] The cuboids were modeled after the experimental geometry and the dielectric function of silver was taken from tabulated literature values.[16] The substrate was modeled as a 15 nm thick Si_3N_4 layer with a lateral rectangular size of 300 × 600 nm. The charge maps in Figure 2b,d were simulated at the mode peak energies derived from simulated EEL spectra (not shown) that correspond well to the experimental data. Starting with the first order modes in Figure 2b, the simulated patterns corroborate our mode assignment. Importantly, the charge maps illustrate that the different patterns of L_1 and L_1' are due to parallel and antiparallel orientation, respectively, of the dipolar edge modes in the two long cuboid edges. We note that the slight differences in experimental and simulated mode energies (compare Figure 2 panel a to panel b and panel c to panel d) are most likely due to deviations of the cuboid geometry from the shape assumed in the simulations as well as due to differences between the dielectric function of silver in the experiment and that used for the simulations.[16]

The simulations thus suggest to interpret the mode patterns as due to the mutual coupling of the edge plasmons (along the long cuboid edge) across the cuboid. Indeed, the simulated charge patterns for L_2, L_2' and L_3, L_3' in Figure 2b confirm this view. In each case, we observe both bonding (lower energy) and antibonding (higher energy) edge modes with energy splittings becoming smaller for higher mode order. The experimental EEL maps for L_2 and L_2' indeed show the corresponding differences in the mode patterns. However, the mode splitting of only 0.04 eV for the L_3 and L_3' modes (simulations) is below the experimental energy resolution. Nevertheless, the corresponding spectrum in Figure 1a (green curve) strongly hints toward mode splitting. For completeness, EEL spectra and maps of the individual and coupled edge modes are shown in Supplementary Figure 3.

EEL spectra acquired on the short cuboid edge and within the cuboid are plotted in Figure 1b. The corresponding EEL maps in Figure 2c illustrate the modes as an edge mode (S_2) and a film mode (F_2) both standing waves of second order. Again, the simulations (Figure 2d) fit well to the experimental data. It is however important to note that the S_2 mode is spectrally very close to L_3, and thus cannot be spectrally separated in the experiment. This explains the appearance of both mode pattern features in the EEL maps of L_3 and L_3' (Figure 2a) and S_2 (Figure 2c). Interestingly, the S_2 mode appears as a single peak in the EEL spectra in both the experimental and simulated data, implying that no coupling between the short cuboid edges takes place. Indeed, this is due to the larger distance in between the short edges (300 nm), as compared to the distance between the long edges (150 nm).

To shed more light on this issue, we simulate the EEL spectra and charge maps for cuboids with varying widths, that is, different distances between the long cuboid edges, thus varying their mutual coupling. For computational restraints, we chose smaller cuboids with a length of 150 nm and a width varied between 150 and 40 nm for a height of 30 nm. In Figure 3, we show density plots of EEL spectra in dependence of the cuboid width (vertical axis). In Figure 3a, the electron beam position is chosen in the middle position of the long cuboid edge. Here, due to symmetry the electron beam can excite both

DOI: 10.1021/acs.nanolett.6b02097
Nano Lett. 2016, 16, 5152−5155

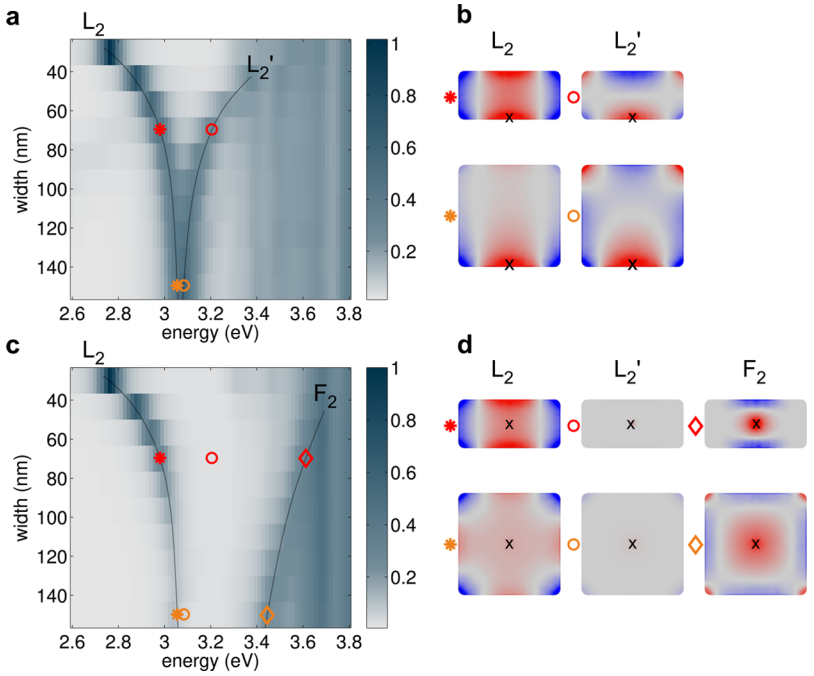

Figure 3. Simulated EEL spectra and surface charge maps of the edge modes L_2, L_2' and the film mode F_2 of a cuboid with a length of 150 nm, a height of 30 nm, and a width varied from 150 to 40 nm. Density plots of the EEL spectra (horizontal axis) as a function of the short cuboid edge length (vertical axis) are shown for electron beam positions (a) in the middle position of the long cuboid edge and (c) in the cuboid center, as indicated by the crosses in the charge density maps in (b,d). The charge density maps were simulated for the values indicated by the orange and red symbols in the density plots in (a,c). The crosses mark the position of the exciting electron beam.

bonding and antibonding edge modes. Decreasing the width from a square to a rectangular footprint, we observe mode splitting into a bonding and an antibonding mode, as confirmed by the charge maps in Figure 3b. On the other hand, for an electron position in the cuboid center only the bonding mode L_2 can be excited, as evident from the absence of the L_2' branch (Figure 3c,d). In this case, however, the film mode F_2 can be effectively excited.

Finally, we experimentally study edge mode splitting as a function of the cuboid length (300−500 nm), keeping width (150 nm) and height (30 nm) constant, as depicted in the transmission electron microscope (TEM) images in Figure 4. The experimental peak positions of the bonding and antibonding modes L_1-L_3 and L_1'-L_2' are plotted as a function of the particle length, together with the spectral positions of the S_2 and F_2 modes (for the corresponding spectra, see Supplementary Figure 1). The latter peaks are not affected by the edge length changes, as expected. In contrast, for the modes along the long cuboid edge we find a decrease in mode energy with increasing length, together with an increased mode energy splitting. This is exemplified with the red lines in Figure 4 for the L_2 and L_2' modes, where the mode splitting energy of 0.22 eV for a cuboid length of 300 nm increases to 0.50 eV for a cuboid length of 500 nm. For any given edge mode order, the mode energy is determined by the edge length. As expected for the mode volume and as illustrated by the surface charge maps in Figure 2, lower order modes (with correspondingly larger wavelengths) show less localized charge distributions. The correspondingly larger mode volume leads to a stronger overlap of the two modes on the long cuboid edges (that are kept at constant distance) and thus to stronger coupling. This in turn gives rise to larger energy splitting for longer particles and lower mode orders. From the data in Figures 3 and 4, it is also evident that for the particle geometries chosen for this study,

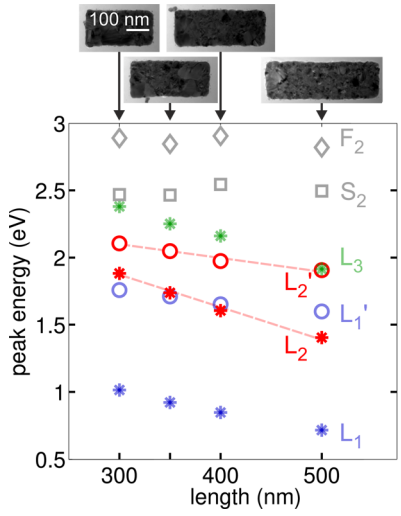

Figure 4. Edge length dependent mode splitting of four cuboids 30 nm high and 150 nm wide with lengths of 300, 350, 400, and 500 nm, as shown in the transmission electron microscope bright field images on top. The energy splitting is exemplified for the L_2 and L_2' modes by the dashed red lines.

effective mode coupling only takes place for the long cuboid axes, as the short axes are too far apart.

In conclusion, we used STEM-EELS together with numerical simulations to study the plasmon mode spectrum of lithographically tailored silver nanocuboids. We identified the pairwise appearance of low-energy peaks as being due to the mutual coupling of opposite edge plasmons, leading to bonding, and antibonding edge modes. This coupled edge mode model straightforwardly explains the mode energies in dependence of the nanoparticle geometry and is thus an

DOI: 10.1021/acs.nanolett.6b02097
Nano Lett. 2016, 16, 5152−5155

effective tool for the understanding and tailoring of plasmonic mode spectra. Besides plasmonic metal systems this model can be useful as well for other material systems as, for example, graphene.[17]

Methods. We prepared silver nanocuboids by electron beam lithography (EBL) in a RAITH e-line system using a poly(methylmetacrylate) resist on a 15 nm thick silicon nitride (Si_3N_4) membrane and a standard silver evaporation and lift-off procedure.[18] The samples were studied in a FEI Tecnai F20 transmission electron microscope with a monochromated 200 keV electron beam of 150 meV energy spread (full width at half-maximum, fwhm). Electron energy loss spectra were recorded in the STEM-EELS mode[9] with an energy dispersion of 0.01 eV/channel in a high-resolution Gatan Imaging Filter equipped with a 2048 × 2048 pixel CCD camera. The energy resolution was further improved by a Richardson-Lucy deconvolution (MathWorks Matlab, deconvlucy function), implemented in a homemade analysis program ("SI analysis tool - A flexible MATLAB tool to analyze spectrum images", available at http://esteem2.eu in the section "Software"). The resulting effective energy resolution was 45 meV (fwhm of the zero-loss peak). Spectrum images were acquired in scan areas ranging from 364 × 212 nm for the smallest cuboid to 589 × 249 nm for the largest cuboids with scan step sizes between 6.1 and 8.3 nm, an acquisition time of 0.1 s per pixel, and a collection semiangle of 9.19 mrad. The EEL maps shown in Figure 2a,c are integrated over an energy range of 100 meV. In addition, the electron micrographs for sample overview shown in the insets of Figure 1a,b are EEL maps integrated over the full energy range of the elastically scattered electrons. The peak energies plotted in Figure 4 were retrieved from fitted Gaussians (see Supplementary Note 2 in ref 7), leading to a fit error below 0.015 eV, which is much smaller than the symbol size.

■ ASSOCIATED CONTENT

Supporting Information

The Supporting Information is available free of charge on the ACS Publications website at DOI: 10.1021/acs.nanolett.6b02097.

Additional figures(PDF)

■ AUTHOR INFORMATION

Corresponding Author

*E-mail: franz.schmidt@uni-graz.at.

Notes

The authors declare no competing financial interest.

SI analysis tool, a flexible MATLAB tool to analyze spectrum images, available at http://esteem2.eu.

■ ACKNOWLEDGMENTS

This work was supported by the FWF SFB NextLite (F4905-N23 and F4906-N23), ESTEEM2 (FP7 project, no. 312483), NAWI Graz, and the Graz Centre for Electron Microscopy (ZFE).

■ REFERENCES

(1) Aizpurua, J.; Hanarp, P.; Sutherland, D. S.; Käll, M.; Bryant, G. W.; García de Abajo, F. J. *Phys. Rev. Lett.* **2003**, *90*, 057401.

(2) Koh, A. L.; Bao, K.; Khan, I.; Smith, W. E.; Kothleitner, G.; Nordlander, P.; Maier, S. A.; McComb, D. W. *ACS Nano* **2009**, *3*, 3015−3022.

(3) Koh, A. L.; Fernández-Domínguez, A. I.; McComb, D. W.; Maier, S. A.; Yang, J. K. W. *Nano Lett.* **2011**, *11*, 1323−1330.

(4) Tong, L.; Wei, H.; Zhang, S.; Li, Z.; Xu, H. *Phys. Chem. Chem. Phys.* **2013**, *15*, 4100−4109.

(5) Prodan, E.; Radloff, C.; Halas, N. J.; Nordlander, P. *Science* **2003**, *302*, 419−422.

(6) Liu, W.; Oulton, R. F.; Kivshar, Y. S. *Sci. Rep.* **2015**, *5*, 12148.

(7) Schmidt, F.-P.; Ditlbacher, H.; Hohenester, U.; Hohenau, A.; Hofer, F.; Krenn, J. R. *Nat. Commun.* **2014**, *5*, 3604.

(8) Bellido, E. P.; Manjavacas, A.; Zhang, Y.; Cao, Y.; Nordlander, P.; Botton, G. A. *ACS Photonics* **2016**, *3*, 428−433.

(9) Jeanguillaume, C.; Colliex, C. *Ultramicroscopy* **1989**, *28*, 252−257.

(10) Nelayah, J.; Kociak, M.; Stéphan, O.; García de Abajo, F. J.; Tencé, M.; Henrard, L.; Taverna, D.; Pastoriza-Santos, I.; Liz-Marzán, L. M.; Colliex, C. *Nat. Phys.* **2007**, *3*, 348−353.

(11) Rocca, M. *Surf. Sci. Rep.* **1995**, *22*, 1−71.

(12) Schmidt, F.-P.; Ditlbacher, H.; Hohenester, U.; Hohenau, A.; Hofer, F.; Krenn, J. R. *Nano Lett.* **2012**, *12*, 5780−5783.

(13) Schmidt, F. P.; Ditlbacher, H.; Hofer, F.; Krenn, J. R.; Hohenester, U. *Nano Lett.* **2014**, *14*, 4810−4815.

(14) Hohenester, U.; Trügler, A. *Comput. Phys. Commun.* **2012**, *183*, 370−381.

(15) Hohenester, U. *Comput. Phys. Commun.* **2014**, *185*, 1177−1187.

(16) Johnson, P. B.; Christy, R. W. *Phys. Rev. B* **1972**, *6*, 4370−4379.

(17) Nikitin, A. Y.; Alonso-González, P.; Vélez, S.; Mastel, S.; Centeno, A.; Pesquera, A.; Zurutuza, A.; Casanova, F.; Hueso, L. E.; Koppens, F. H. L.; Hillenbrand, R. *Nat. Photonics* **2016**, *10*, 239−243.

(18) Hohenau, A.; Ditlbacher, H.; Lamprecht, B.; Krenn, J. R.; Leitner, A.; Aussenegg, F. R. *Microelectron. Eng.* **2006**, *83*, 1464−1467.

DOI: 10.1021/acs.nanolett.6b02097
Nano Lett. 2016, 16, 5152−5155